

# Formability investigation of two advanced high-strength steels: conventional versus high total elongation 780 MPa grades

Francislaynne Lages Dias<sup>1\*</sup>   
 Fabrício Moreira Cerqueira<sup>1</sup>   
 Flávio José Saraiva Rodrigues<sup>2</sup>   
 Marden Valente de Souza<sup>2</sup>   
 Jetson Ferreira Lemos<sup>2</sup>   
 Roan Sampaio de Souza<sup>2</sup>   
 Gabriel Godinho Alves<sup>1</sup>   
 Felipe Pereira Finamor<sup>2</sup>   
 Fabiano José Fabri Miranda<sup>1</sup> 

## Abstract

Advanced High-Strength Steels are widely employed in the automotive industry to reduce vehicle mass without compromising structural integrity and safety requirements. However, the limited formability of these materials imposes significant constraints on forming processes. This study compares the formability of an AHSS with a minimum tensile strength of 780 MPa, industrially produced through two distinct thermomechanical processing routes: conventional and optimized with high total elongation. The samples were characterized in terms of microstructure, mechanical behavior and formability. The results indicate that the optimized condition, featuring greater homogeneity, higher volume fractions of bainite and retained austenite, and increased elongation, exhibited a 20% increase in  $FLC_0$  and 55% improvement in edge stretchability, demonstrating substantial enhancements in both global and local formability. Numerical simulation of the stamping process showed a significant reduction in failure due to fracture. These findings were validated at the industrial scale, where the rework rate of stamped parts was reduced from 30–40% to nearly zero. Such results reinforce the importance of microstructural control as a key tool to enable the application of AHSS materials in automotive components with complex geometries.

**Keywords:** AHSS; 780 MPa Grade; Microstructure; Formability.

## 1 Introduction

Advanced high-strength steels (AHSS) have been widely adopted in the automotive industry due to their favourable combination of high mechanical strength and good formability: key attributes for meeting safety, energy efficiency, and weight reduction requirements. Microstructural factors such as martensite distribution and volume fraction, grain size, presence of secondary phases, and crystallographic texture directly influence mechanical behaviour and, consequently, formability.

The formability of AHSS, particularly in processes involving complex geometries, is often limited by intrinsic microstructural characteristics. Martensite, a phase with high hardness and low toughness, distributed as islands within a ductile ferritic matrix, is essential for achieving high strength but also acts as a potential site for crack nucleation under severe deformation. Mechanical and plastic incompatibility

at martensite-ferrite interfaces promotes localized stress concentrations, favouring crack initiation and propagation. This behaviour compromises both local ductility and global formability, restricting performance in applications requiring high deformation capacity [1]. In terms of microstructure, it is reported that the presence of bainite constituent in dual-phase steels enhances edge stretchability (HER) compared to ferrite-martensite steels, as voids tend to initiate in bainite at higher strains than in martensite [2]. Furthermore, global formability, assessed by the Forming Limit Curve (FLC), strongly depends on the TRIP effect and a uniform distribution of hard phases. Additionally, a higher coefficient of normal anisotropy and positive strain-rate sensitivity contribute to excellent pre- and post-uniform elongation, resulting in superior global formability [3]. Figure 1 illustrates a

<sup>1</sup>ArcelorMittal Vega, São Francisco do Sul, SC, Brasil.

<sup>2</sup>ArcelorMittal Tubarão, Vitória, ES, Brasil.

\*Corresponding author: francislaynne.dias@arcelormittal.com.br

E-mails: fabricio.cerqueira@arcelormittal.com.br; flavio.rodrigues@arcelormittal.com.br; marden.souza@arcelormittal.com.br; jetson.ferreira@arcelormittal.com.br; roan.souza@amcontratos.com.br; gabriel.godinho@arcelormittal.com.br; felipe.finamor@arcelormittal.com.br; fabiano.jf.miranda@amcontratos.com.br



2176-1523 © 2026. Dias et al. Published by ABM. This is an Open Access article distributed under the terms of the Creative Commons Attribution license (<https://creativecommons.org/licenses/by/4.0/>), which permits unrestricted use, distribution, and reproduction in any medium, provided the original work is properly cited.

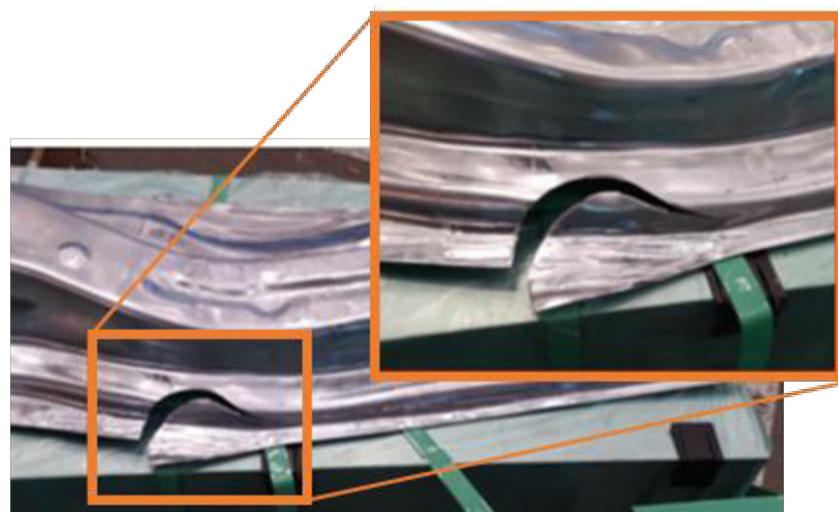


**Figure 1.** Fracture in an AHSS stamped component.

stamped AHSS component that fractured during forming, highlighting limitations in regions of geometric complexity.

This study aims to compare the formability of an AHSS with a minimum tensile strength of 780 MPa, produced through two industrial thermomechanical processing routes: a conventional and an optimized designed to achieve high total elongation. These routes promote microstructural changes intended to improve formability, such as a fine and homogeneous distribution of hard phases and retained austenite, as well as a higher bainite content. Correlations will be established between microstructural characteristics, mechanical properties (yield strength, uniform elongation, strain-hardening exponent), and formability indicators: both global (FLC) and local (edge stretchability measured by HER). Based on mechanical data, a numerical simulation of the stamping process of an automotive rail will be performed and compared with results from components formed under industrial conditions.

## 2 Materials and methods

In this study, flat sheets of an AHSS with a minimum tensile strength of 780 MPa, hot-dip galvanized (HDG-GI), and 1.60 mm in thickness were evaluated. Table 1 presents the nominal chemical composition of these steels.

The steels were industrially produced in two conditions: the conventional one (AHSS) and another aimed at achieving high total elongation (AHSS HTE), through soaking temperature and line speed adjustments. Table 2 presents the mechanical property requirements under uniaxial tensile testing.

The samples microstructures were analyzed using scanning electron microscopy (SEM), optical microscope (OM) and electron backscatter diffraction (EBSD), in the longitudinal section relative to the rolling direction, at 4000x

**Table 1.** Limit values of chemical composition (% weight)

C	Si	Mn	P	S	Cr+Mo	Nb+Ti	Al	Cu	B
0.18	0.80	2.5	0.05	0.01	1.40	0.15	1.00	0.20	0.005

**Table 2.** Mechanical property requirements in longitudinal tensile testing

Yield Strength [Mpa]	Ultimate Strength [MPa]	Total Elongation [%]
420-550	≥ 780	≥ 15

magnification and a scan step of 0,1  $\mu$ m. A qualitative phase analysis was performed based on EBSD scans.

Tensile properties were determined according to ISO 6892-1 [4], using sheet-type specimens extracted in the longitudinal direction relative to rolling. The gauge length for elongation measurement was 80 mm.

Hole Expansion Ratio (HER) tests were conducted in accordance with ISO 16630 [5], using square blanks of 100 mm per side and a punch with 60° conicity, until a crack appeared at the edge of a central hole previously made with a 10 mm diameter. The holes were produced by punching, with 12% clearance and burrs positioned against the punch during testing. The test continues until a through-thickness crack appears. The HER value was calculated using the Equation 1 and reported as the average of five valid specimens.

$$HER = \frac{d_f - d_0}{d_0} \times 100 \quad (1)$$

Forming Limit Curves (FLCs) were obtained based on ArcelorMittal's empirical-analytical model [6]. The data obtained in this study were used to construct the material model for numerical simulation of the stamping process of a rail component, manufactured with both steels. The simulation results were compared with those obtained from physical stamping of the same part.

### 3 Results and discussion

The typical aspect of the microstructures is shown in Figure 2. A microstructure composed of a ferritic matrix and a second phase consisting of martensite and bainite can be observed, with greater homogeneity in the AHSS HTE (Figure 2c,d).

The presence of retained austenite was also observed (using Klemm etching to differentiate austenite white phase from ferrite and bainite in blue and martensite in brown, Figure 3), being twice higher in AHSS HTE (Figure 3b). In this steel, the austenite is thinner and homogeneously distributed, with appearing both as isolated islands and as needles and particles within packets that resemble bainite or tempered/partitioned martensite. In contrast, in the conventional steel, austenite appears in small amounts as isolated islands at the grain boundaries of the matrix.

A homogeneously distributed austenite, especially when present as thin films or small particles within bainitic

or martensitic matrices, can significantly enhance ductility. This is primarily due to the Transformation-Induced Plasticity (TRIP) effect, where retained austenite transforms into martensite under strain, absorbing energy and delaying necking. In contrast, when austenite is present only in small, isolated islands at grain boundaries, its contribution to ductility is limited [7].

Phase analysis obtained via EBSD (Figure 4) indicated that the AHSS HTE also contains a bainite fraction three times higher than that of the conventional AHSS.

Table 3 presents the results obtained from uniaxial tensile testing. An increase in yield strength is observed in the AHSS HTE steel compared to the conventional grade, attributed to the formation of bainite, a high-strength constituent, at the expense of ferrite, which is a softer phase. An increase in both uniform and total elongation is also noted.

The behavior of the instantaneous strain hardening exponent as a function of the strain applied to the material during the tensile test is illustrated in Figure 5. The peak of

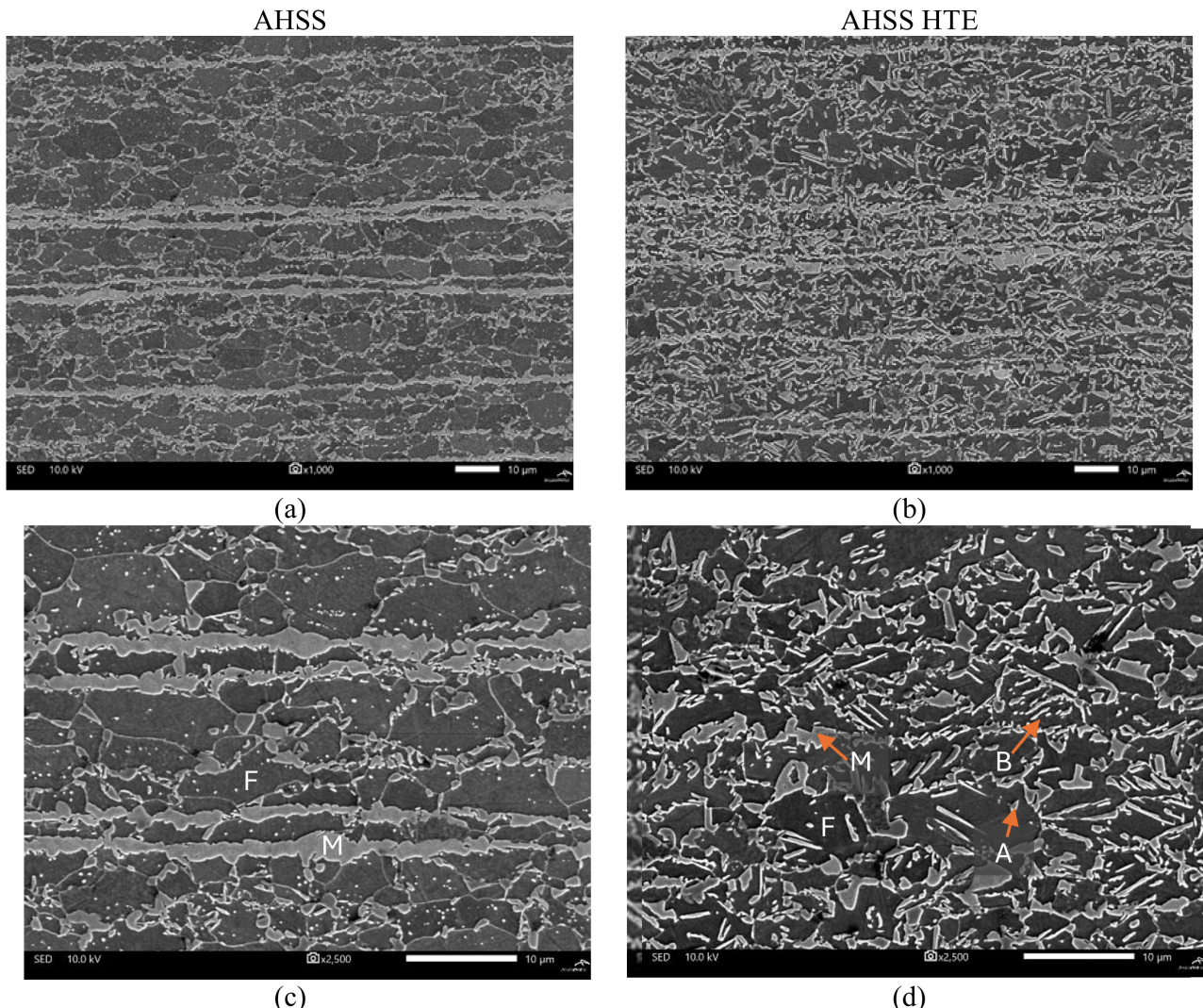


**Figure 2.** Microstructural features of the samples as observed by SEM of AHSS with (a) 1.000x, (c) 2.500x magnification and AHSS HTE with (b) 1000x, (d) 2500x magnification.

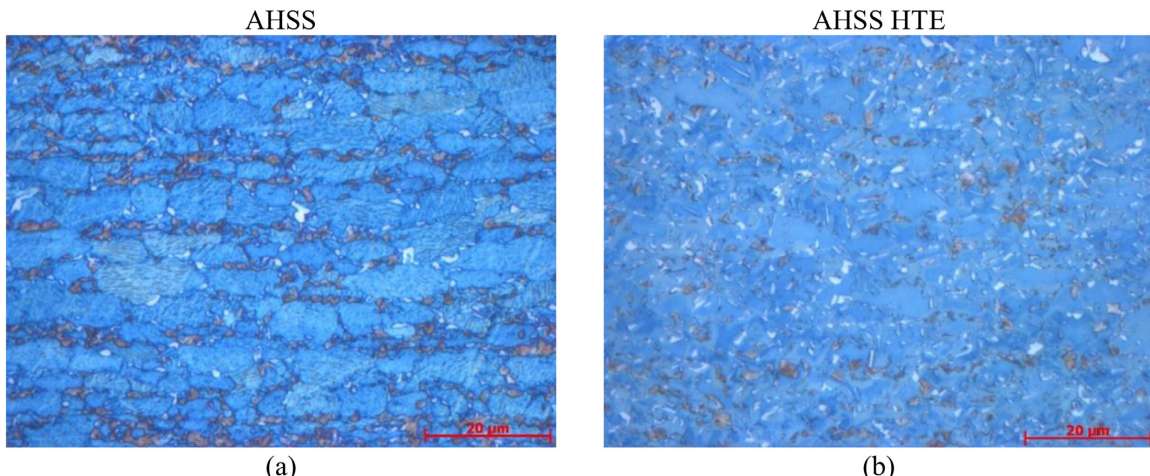


Figure 3. Microstructural features of the samples as observed by OM of (a) AHSS and (b) AHSS HTE with 1000x magnification.

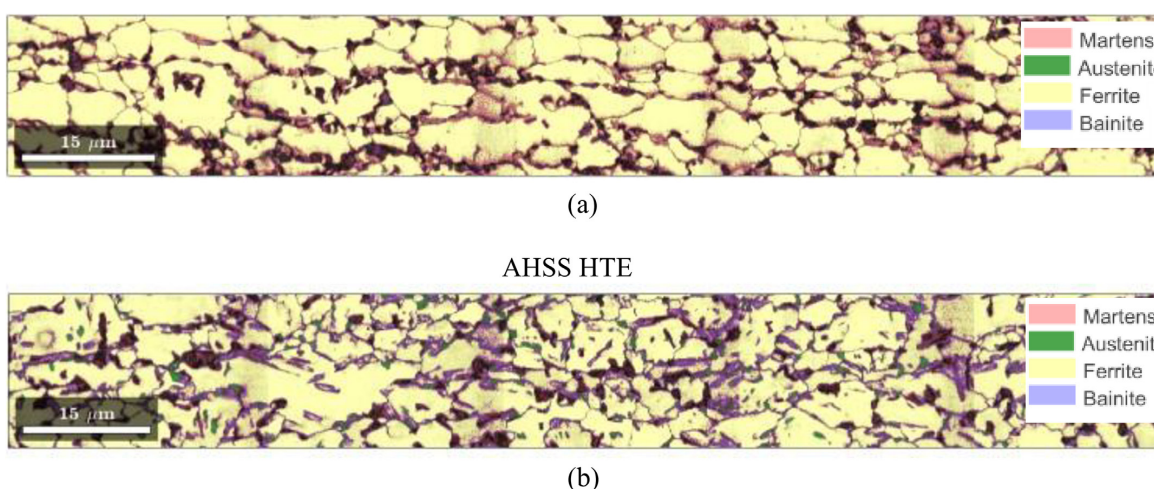


Figure 4. Phase segmentation carried out using EBSD data processed with Matlab of (a) AHSS and (b) AHSS HTE with 4000x magnification.

Table 3. Mechanical properties obtained from tensile testing in the longitudinal direction

	Yield	Ultimate	Uniform	Total
	Strength [MPa]	Strength [MPa]	Elongation [%]	Elongation [%]
AHSS	442	806	12.4	17.9
AHSS HTE	482	817	16.4	23.4

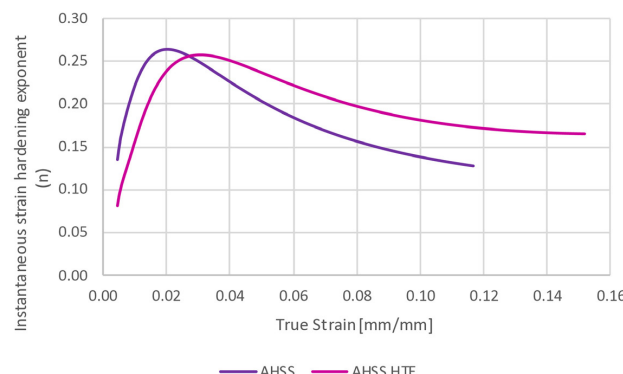


Figure 5. Instantaneous strain hardening exponent.

the strain hardening exponent ( $n$ -value) occurs at different true strain levels for the two materials: approximately 0.02 for AHSS and around 0.03 for AHSS HTE.

This indicates that the AHSS HTE retains its strain hardening capability over a broader strain range, which can be advantageous in forming processes by enhancing formability and delaying localized necking.

Once the retained austenite also transforms to martensite typically at this stage, the local transformation of retained austenite increases the dislocation density, creates additional nonuniformity of deformation and hence the rate of strain hardening [8].

Both materials exhibit a typical decline in the  $n$ -value with increasing strain, reflecting the progressive reduction in strain hardening capacity as deformation proceeds. However, AHSS HTE consistently maintains slightly higher  $n$ -values throughout the deformation range, suggesting improved resistance to strain softening and potentially better mechanical stability during forming operations.

These enhancement in mechanical properties is a result of a more homogeneous microstructure, with an

optimized presence of bainite and retained austenite in the AHSS HTE steel. This is consistent with findings by Zhao et al. [9], who demonstrated that microalloying and bainitic refinement significantly enhance strength and ductility in dual-phase steels.

Microstructural factors also influenced the material's behavior in terms of both global and local formability.

An increase in global formability, evaluated through the forming limit curve (FLC) raised to necking, can be observed in Figure 6. The lowest point of the curve,  $FLC_0$ , for the AHSS HTE steel showed a 20% increase compared to the conventional material, reflecting the improvement in the material's uniform elongation.

The increase in local formability, measured by the Hole Expansion Ratio (HER) test, was even more significant, showing a 55% gain in edge stretchability – HER increased from 18% to 28%, as illustrated in Figure 7. Such a property in high-strength steels is reported to depend on several factors, such as the hardness difference between phases, the volume fraction of retained austenite present in the microstructure and its stability, the uniform elongation, among others. In this case, the presence of bainite reduces the hardness gradient between the softer ferrite and the harder martensite phases. The pronounced contrast in mechanical properties between ferrite and martensite typically leads to high hardness gradients and plastic incompatibilities at their interfaces, which promote crack nucleation, particularly in trimmed edge regions. By mitigating these gradients, bainite enhances edge stretchability and contributes to the superior performance of AHSS HTE compared to the conventional grade. Additionally, greater microstructural homogeneity and austenite content further supports improved edge formability. Similar improvements in edge formability were reported by Zhou et al.[10] when comparing 780 MPa AHSS steels with different phase distributions.

Based on the material data, the numerical stamping simulation model for the customer's component was calibrated (Figure 8 a,b). A reduction in crack incidence was observed when simulation was conducted with AHSS HTE (Figure 8b), when compared to conventional AHSS (Figure 8a).

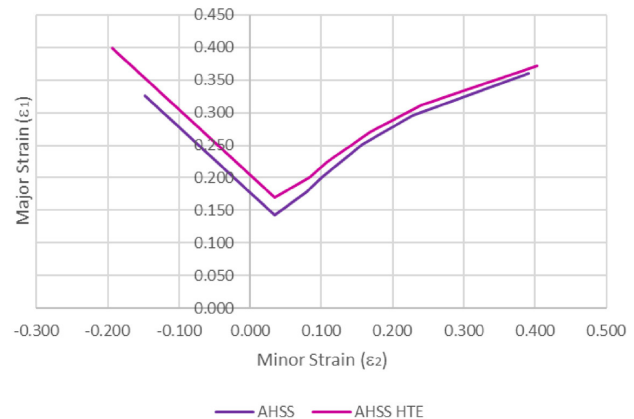


Figure 6. Forming Limit Curve.



Figure 7. Hole Expansion Ratio.

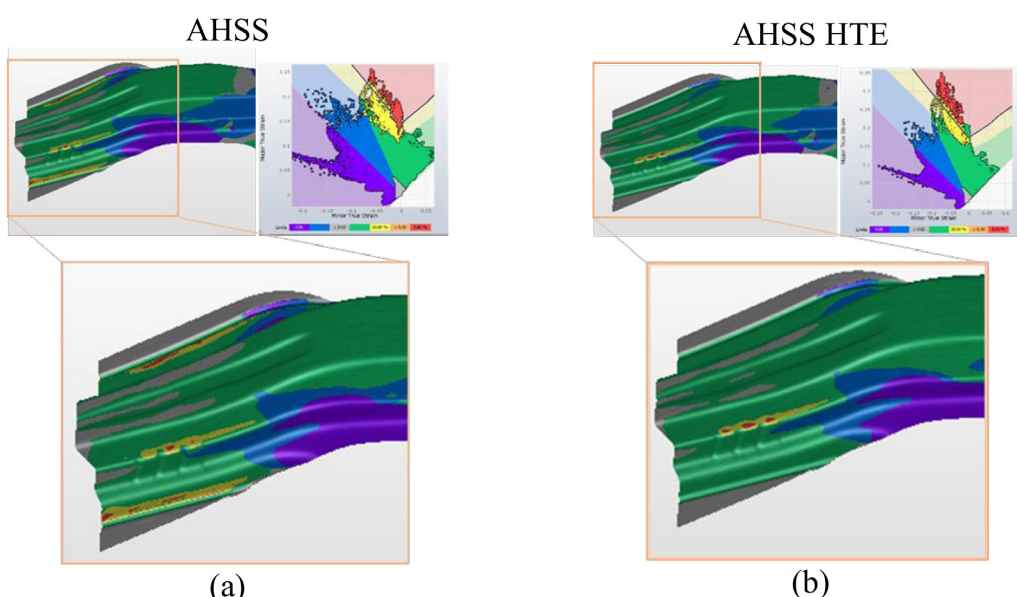
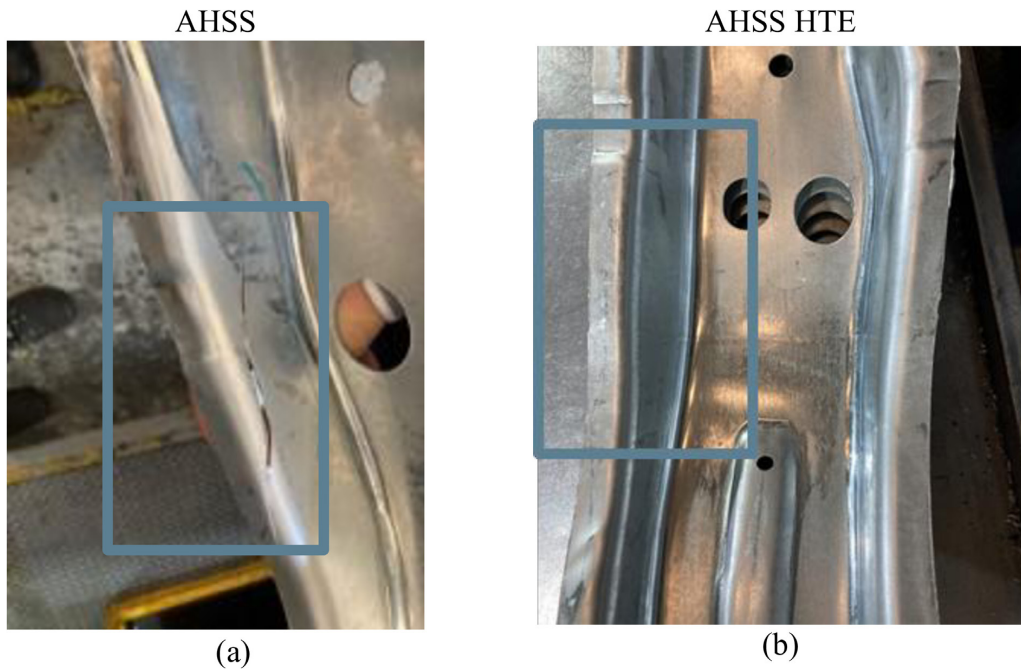


Figure 8. Numerical stamping simulation of (a) AHSS and (b) AHSS HTE.



**Figure 9.** Industrial part after the forming stage of (a) AHSS and (b) AHSS HTE.

In Figure 9 an image of the stamped part produced from both steels is presented, clearly showing visible cracks from stamping in component formed with AHSS (Figure 9a) and the absence of cracks in the component formed with AHSS HTE (Figure 9d).

Up to the conclusion of this study, the customer reported the successful stamping of 1.050 parts without any occurrence of fractures. Furthermore, the rework rate, previously ranging from 30% to 40%, was eliminated.

#### 4 Conclusion

The microstructure, uniaxial tensile behavior, and formability of an AHSS with high total elongation (HTE) were evaluated in comparison to conventional AHSS of

the same thickness. AHSS HTE exhibited enhanced strain hardening behavior over a broader strain range compared to the conventional grade, resulting in gains of 20% in global formability. This steel also shows 55% increase in local formability. These characteristics enables stamping of components with more complex geometries.

In its application, a significant reduction in stamping failures was observed, validated by numerical simulations and industrial trials. Preliminary results indicate a significant reduction in rework, on the order of 40% to zero, leading to increased productivity and reduced costs.

The superior performance of AHSS HTE was attributed to its greater microstructural homogeneity, with an optimized presence of bainite and retained austenite, highlighting the importance of microstructural control in the application of advanced steels in the automotive industry.

#### References

- 1 Ren Y, Li S, Feng S, Li Y, Yuan C. In Situ EBSD Observation and Numerical Simulation of Microstructure Evolution and Strain Localization of DP780 Dual-Phase Steel. *Materials (Basel)*. 2025;18(2):426. <https://doi.org/10.3390/ma18020426>.
- 2 Paul KP. A critical review on hole expansion ratio. *Materialia*. 2020;9:100566. <https://doi.org/10.1016/j.mtla.2019.100566>.
- 3 Paul KP. Controlling factors of forming limit curve: a review. *Advances in Industrial and Manufacturing Engineering*. 2021;2:100033. <https://doi.org/10.1016/j.aime.2021.100033>.
- 4 International Organization for Standardization. ISO 6892-1:2019 - Metallic materials — Tensile testing — Part 1: Method of test at room temperature. Geneva: ISO; 2017.

- 5 International Organization for Standardization. ISO 16630:2017 - Metallic materials — Sheet and strip — Hole expanding test. Geneva: ISO; 2017.
- 6 Cayssials F, Lemoine X. Predictive model of FLD (Arcelor model) upgraded to UHSS Steels. In: Proceedings of the International Deep Drawing Research Group; 2005 June 20-22; Besançon, France. Besançon: IDDRG; 2005.
- 7 Aranzabal J, Gutierrez I, Rodriguez-Ibabe JM, Urcola JJ. Influence of the amount and morphology of retained austenite on the mechanical properties of an austempered ductile iron. Metallurgical and Materials Transactions. A, Physical Metallurgy and Materials Science. 1997;28(6):1143-1156. <https://doi.org/10.1007/s11661-997-0280-6>.
- 8 Fonstein N. Dual-phase steels. In: Rana R, Singh SB, editors. Automotive steels – design, metallurgy, processing and applications. Sawston: Woodhead Publishing; 2017. p. 169–216. <https://doi.org/10.1016/B978-0-08-100638-2.00007-9>.
- 9 Zhao J, He K, Guo Y, Fan X, Yan B, Lu X, et al. Evolution of microstructure and mechanical properties in dual-phase steel containing Ce and Nb. Journal of Materials Engineering and Performance. 2024;33(18):9829-9839. <https://doi.org/10.1007/s11665-023-08627-5>.
- 10 Zhou L, Xue R, Cao X, Wen C. Study on the differences in microstructure, mechanical properties, and deformation mechanism between DH and DP steels. Iron Steel Vanadium Titanium. 2023, 44(6): 186-191. <https://doi.org/10.7513/j.issn.1004-7638.2023.06.026>

Received: 30 Set. 2025

Accepted: 28 Dec. 2025

Editor-in-charge:

André Luiz Vasconcellos da Costa e Silva 